

Sub-millimeter brightness of early star-forming galaxies

Hideobu Yajima^{1*}, Masayuki Umemura², Masao Mori²

¹*Department of Astronomy and Astrophysics, Pennsylvania State University, 525 Davey Lab, University Park, PA 16802, USA*

²*Center for Computational Sciences, University of Tsukuba, Tsukuba 305-8577, Japan*

Accepted ??; Received ??; in original form ???

ABSTRACT

Based on a three-dimensional model of an early star-forming galaxy, we explore the evolution of the sub-millimeter brightness. The model galaxy is employed from an ultra-high-resolution chemodynamic simulation of a primordial galaxy by Mori & Umemura, where the star formation rate (SFR) is $\sim 10 \text{ M}_{\odot} \text{ yr}^{-1}$ at $t_{\text{age}} \lesssim 0.3 \text{ Gyr}$ and several $\text{M}_{\odot} \text{ yr}^{-1}$ at $t_{\text{age}} > 0.3 \text{ Gyr}$. The former phase well reproduces the observed properties of Lyman alpha emitters (LAEs) and the latter does Lyman break galaxies (LBGs). We solve the three-dimensional radiative transfer in the clumpy interstellar media in this model galaxy, taking the size distributions of dust grains into account, and calculate the dust temperature as a function of galactic evolutionary time. We find that the clumpiness of interstellar media plays an important role for the sub-millimeter brightness. In the LAE phase, dust grains are concentrated on clumpy star-forming regions that are distributed all over the galaxy, and the grains can effectively absorb UV radiation from stars. As a result, the dust is heated up to $T_{\text{dust}} \gtrsim 35 \text{ K}$. In the LBG phase, the continuous supernovae drive dust grains far away from star-forming regions. Then, the grains cannot absorb much radiation from stars, and becomes into a cold state close to the CMB temperature. Consequently, the dust temperature decreases with the evolutionary time, where the mass-weighted mean temperature is $T_{\text{dust}} = 26 \text{ K}$ at $t_{\text{age}} = 0.1 \text{ Gyr}$ and $T_{\text{dust}} = 21 \text{ K}$ at $t_{\text{age}} = 1.0 \text{ Gyr}$. By this analysis, it turns out that the sub-millimeter brightness is higher in the LAE phase than that in the LBG phase, although the dust-to-gas ratio increases monotonically as a function of time. We derive the spectral energy distributions by placing the model galaxy at a given redshift. The peak flux at $850 \mu\text{m}$ is found to be $S_{850} \sim 0.2 - 0.9 \text{ mJy}$ if the model galaxy is placed at $6 \geq z \geq 2$. This means that ALMA can detect an early star-forming galaxy with SFR of $\sim 10 \text{ M}_{\odot} \text{ yr}^{-1}$ by less than one hour integration with 16 antennas.

Key words: radiative transfer – ISM: dust, extinction – galaxies: evolution – galaxies: formation – galaxies: high-redshift – methods: numerical

1 INTRODUCTION

Exploring the properties of early star-forming galaxies is one of key themes to elucidate the galaxy formation process. The fashion of star formation in galaxies can significantly change dust properties. In young galaxies, type-II supernovae create dust, and also change the dust size and component (Dwek 1998; Todini & Ferrara 2001; Bianchi & Schneider 2007; Nozawa, Kozasa, & Habe 2006; Nozawa et al. 2007). In addition, UV radiation from young stars is effectively absorbed by dust and therefore determines the temperature of dust grains. Besides, the dust can affect the star forma-

tion efficiency itself via hydrogen molecule formation and the cooling by thermal emission. Accordingly, dust properties such as amount, temperature, size and composition should tightly correlate with the star formation history. Hence, understanding the dust properties is a significant issue in the study of galaxy evolution.

So far, the sub-millimeter (sub-mm) flux from distant galaxies has been detected at redshifts of $0.3 - 4$. These galaxies are called sub-mm galaxies (SMGs) (e.g., Smail, Ivison, & Blain 1997; Hughes et al. 1998; Barger et al. 1998; Eales et al. 1999; Ivison et al. 2000; Daddi et al. 2009). However, the observed galaxies are limited to extremely luminous starburst galaxies, where the star formation rate (SFR) is $\sim 1000 \text{ M}_{\odot} \text{ yr}^{-1}$, from the restriction by the detection limit of the facility (e.g., Borys et al.

* E-mail: yuh19@psu.edu(HY); umemura@ccs.tsukuba.ac.jp(MU); mmori@ccs.tsukuba.ac.jp(MM)

2003; Greve et al. 2004; Chapman et al. 2005; Laurent et al. 2005; Coppin et al. 2006; Bertoldi et al. 2007; Perera et al. 2008; Scott et al. 2008; Weiß et al. 2009; Austermann et al. 2010; Eales et al. 2010; Hatsukade et al. 2011). Hence, the dust properties in normal star-forming galaxies ($\text{SFR} \lesssim 100 \text{ M}_\odot \text{ yr}^{-1}$) at high redshifts (which mean $z \gtrsim 3$ in this paper) have not been hitherto understood well.

Recently, some observations are dedicated to detect the sub-mm flux from early star-forming galaxies ($\text{SFR} \sim 0.1 - 100 \text{ M}_\odot \text{ yr}^{-1}$) like Lyman alpha emitters (LAEs) and Lyman break galaxies (LBGs) by using newly developed facilities (Tamura et al. 2009; Stanway et al. 2010). Although Tamura et al. (2009) did not detect notable sub-mm flux from LAEs and LBGs in the SSA22 region within the detection limit of $S_{1100} \sim 2 \text{ mJy}$, they discovered sub-mm sources in the vicinity of LAEs. Stanway et al. (2010) showed that the upper-limit of sub-mm flux for LBGs at $z \sim 5$ is $S_{870} < 0.85 \text{ mJy}$ from stacked data. Hence, with recent sub-mm telescopes (e.g. Hershel, AzTEK), it seems very difficult to detect sub-mm flux from high- z star-forming galaxies with $\text{SFR} < 100 \text{ M}_\odot \text{ yr}^{-1}$. Moreover, the determination of dust temperature is a hard task in the observational study, because it requires the flux data at many wavelengths in sub-mm band. Hence, one often assumes the dust temperature to speculate spectral energy distributions (SED). Then, the estimation of L_{IR} by integrating speculated SED suffer from the uncertainty of the assumed dust temperature. The uncertainty leads to the misestimation of SFR and dust amount. A theoretical model may help to relate the observed sub-mm flux with the dust properties in star-forming galaxies. Such attempts have been made by several authors (e.g., Takagi, Vansevicius, & Arimoto 2003; Dayal, Hirashita, & Ferrara 2010). Takagi et al. (2003) constructed an SED model of dusty star-forming galaxies by solving the radiative transfer in spherical symmetry. Dayal et al. (2010), based on cosmological SPH simulations, employed homogeneous distributions of stars and dust in an identified LAE. Recently, Mori & Umemura (2006) have shown through ultra-high-resolution numerical simulations that interstellar media in early star-forming galaxies become quite clumpy as a result of multiple supernovae. Hence, to construct the SED for early star-forming galaxies, it is imperative to solve three-dimensional radiative transfer in clumpy interstellar media.

Here, we theoretically explore the dust amount and temperature in star-forming galaxies by solving three-dimensional radiative transfer, based on a chemodynamic simulation of a primordial galaxy by Mori & Umemura (2006). Since the model galaxy well reproduces the observed properties of Lyman alpha emitters (LAEs) at $t_{\text{age}} \lesssim 0.3 \text{ Gyr}$ and Lyman break galaxies (LBGs) at $t_{\text{age}} > 0.3 \text{ Gyr}$, we can predict the sub-mm brightness in the LAE and LBG phases in early star-forming galaxies. In the present analyses, the cosmological parameters are assumed to be $H_0 = 70 \text{ km s}^{-1} \text{ Mpc}^{-1}$, $\Omega_{\text{M}} = 0.3$ and $\Omega_{\Lambda} = 0.7$. In §2, the model and numerical method are described. In §3, the results on dust properties in early star-forming galaxies are presented. In §4, the detectability by ALMA is discussed. §5 is devoted to the summary.

2 MODEL & METHOD

2.1 Model galaxy

Our model galaxy is a supernova-dominated star-forming galaxy simulated by an ultra-high-resolution (1024^3 fixed Cartesian grids) chemodynamics calculation coupled with the collisionless dynamics of star particles. The simulation pursues the early evolution ($< 2 \times 10^9$ years) of a primeval galaxy as an assemblage of sub-galactic condensations of $5.0 \times 10^9 \text{ M}_\odot$, building up a system with the total mass of 10^{11} M_\odot [see Mori & Umemura (2006) for the simulation details].

The star formation rate (SFR) of the model galaxy is $11 \text{ M}_\odot \text{ yr}^{-1}$ at $t_{\text{age}} = 0.1 \text{ Gyr}$, $10 \text{ M}_\odot \text{ yr}^{-1}$ at $t_{\text{age}} = 0.3 \text{ Gyr}$, $8 \text{ M}_\odot \text{ yr}^{-1}$ at $t_{\text{age}} = 0.5 \text{ Gyr}$, and $5 \text{ M}_\odot \text{ yr}^{-1}$ at $t_{\text{age}} = 1 \text{ Gyr}$. The metal and dust in the galaxy is enriched by the continuous type II supernovae due to vigorous star formation, and exhibits complex inhomogeneous dust distributions (figure 1 in Yajima et al. 2009).

According to the Lyman α luminosity, the early evolutionary stage is divided into two phases: one is the LAE-phase ($t_{\text{age}} \lesssim 0.3 \text{ Gyr}$) and the other is the LBG-phase ($t_{\text{age}} > 0.3 \text{ Gyr}$). Most of Lyman α emission comes from the cooling radiation by interstellar gas, and the luminosity reaches $2.0 \times 10^{43} \text{ erg s}^{-1}$ at $t_{\text{age}} = 0.1 \text{ Gyr}$ and $1.6 \times 10^{43} \text{ erg s}^{-1}$ at $t_{\text{age}} = 0.3 \text{ Gyr}$, respectively. They nicely match the observed luminosity of LAEs and also well resemble LAEs with respect to other properties. At $t_{\text{age}} \geq 0.5 \text{ Gyr}$, the Lyman α luminosity quickly declines to several $10^{41} \text{ erg s}^{-1}$ that is lower than the detection limit, and the SED is dominated by stellar continuum. This phase appears like LBGs. The model galaxy at this phase has stellar age ($\sim 2 - 6 \times 10^8 \text{ yr}$) and mass ($\sim 6 - 9 \times 10^9 \text{ M}_\odot$) similar to typical LBGs at $z \sim 3$, while it is older and more massive than typical LBGs at $z \gtrsim 5$ (Verma et al. 2007). On the other hand, a part of LBGs at $z \gtrsim 5$ have been detected by *Spitzer* IRAC, and show the similar age and mass to our model galaxy (Eyles et al. 2007; Stark et al. 2009). Therefore, our model galaxy at a later phase is probably corresponding to typical LBGs for $z \sim 3$, and a massive subset of LBGs for $z \gtrsim 5$.

2.2 Radiative transfer

The radiation from young stars propagates in the highly inhomogeneous interstellar media containing dust. We compute the three-dimensional radiative transfer (RT) of stellar radiation to derive the dust temperature. The RT calculations are done as the post-processing for each evolutionary stage of model galaxy. For the purpose, the data of the hydrodynamic simulations are coarse-grained into 128^3 Cartesian grids.

The RT scheme used in this paper is the Authentic Radiation Transfer (ART) method which is originally developed by Nakamoto, Umemura, & Susa (2001). The procedure is basically the same as that in Yajima et al. (2009); Yajima, Choi, & Nagamine (2011). Our ART method is based on the *long-characteristic* method. Usually, the *short-characteristic* method is computationally less costly than the long-characteristic method, by an order of N which is a grid number in the linear dimension. However, the short-characteristic method suffers from numerical diffusion effect.

The ART method is devised to reduce the computational cost to a level similar to the short-characteristic method with keeping the accuracy equivalent to the long-characteristic method. Hence, the present method allows us to calculate the transfer of radiation from a large number of sources.

In this work, the RT equation is solved along 16384 rays with uniform angular resolution from each star particle. The number of star particles is $3 - 8.5 \times 10^4$. Hence, we carry out the RT calculation for $\sim 10^{8-9}$ rays for each snapshot. We map individual star particles to nearest grids, and set radiation rays in an isotropic fashion from each star particle.

2.3 Dust model

We distribute the interstellar dust in proportion to the metallicity, assuming the size distribution of $dn_d/da_d \propto a_d^{-3.5}$ (Mathis, Rumpl, & Nordsieck 1977), where a_d is the radius of a dust grain. We suppose the grain size in the range of $0.1 - 1.0 \mu\text{m}$ as our fiducial model. The dust mass in a cell is calculated by a following simple relation between metallicity and dust (Draine et al. 2007),

$$m_d = 0.01 m_g \frac{Z}{Z_\odot}, \quad (1)$$

where m_d , m_g , and Z are the dust mass, gas mass, and metallicity in a cell. The density in a dust grain is assumed to be that of silicate-like grains, 3 g cm^{-3} . The optical depth by dust is given by

$$d\tau_{\text{dust}} = \int Q(a_d, \nu) \pi a_d^2 \left(\frac{dn_d}{da_d} \right) da_d d\nu, \quad (2)$$

where $Q(a_d, \nu)$ and n_d are the absorption coefficient factor and the grain number density, respectively. We adopt the Q -value of silicate grain derived in Draine & Lee (1984).

Of course, there are some options for the dust model. The present dust model is motivated by the supernova dust model in Nozawa et al. (2007). In their model, the small dust grains of $\lesssim 0.01 \mu\text{m}$ are readily destroyed in shock wave, so that the typical size becomes $\sim 0.1 \mu\text{m}$. On the other hand, Todini & Ferrara (2001) pointed out that the typical size could be reduced to $\sim 0.01 \mu\text{m}$ for the first grains in the early universe. The number density of dust grains increases with decreasing dust size for the constant amount of dust, while the absorption cross section decreases with the dust size. In Figure 1, the extinction per unit dust mass is compared between $\sim 0.14 \mu\text{m}$ and $\sim 0.01 \mu\text{m}$ dust. As seen in Figure 1, the absorption efficiency does not change appreciably with changing the dust size. Therefore, the infrared luminosity and dust temperature are not so sensitive to the dust size. Actually, in a test calculation for $0.01 \mu\text{m}$ dust, the temperature decreases by just a few K. The difference in the peak flux at $850 \mu\text{m}$ is a few per cent, because the peak of thermal emission shifts toward $850 \mu\text{m}$ with decreasing temperature.

On the other hand, the Calzetti's law

$$\frac{A_\lambda}{A_V} = \begin{cases} 0.657(-1.857 + 1.040/\lambda) + 1 & \text{for } 0.63 \mu\text{m} \leq \lambda \leq 2.20 \mu\text{m} \\ 0.657(-2.156 + 1.509/\lambda - 0.198/\lambda^2 + 0.011/\lambda^3) + 1 & \text{for } 0.12 \mu\text{m} \leq \lambda < 0.63 \mu\text{m}, \end{cases} \quad (3)$$

(Calzetti et al. 2000) is frequently used for dust extinction in local galaxies. In Figure 2, the extinction curve of our dust model is compared to the Calzetti's law. Our model is somewhat flatter than the Calzetti's law in UV-optical range. However, even if we use Calzetti's extinction curve, the infrared luminosity does not significantly change from our model. Actually, by a test calculation, we find that the relative difference is twenty per cent for IR luminosity, and the difference in dust temperature is \sim a few K.

2.4 Radiative equilibrium

We evaluate the dust temperature T_{dust} by solving the radiative equilibrium between heating by photo-absorption (Γ) and cooling by thermal emission (Λ), which are given by

$$\begin{aligned} \Gamma &= \int \int 4\pi J_\nu Q(a_d, \nu) \pi a_d^2 \frac{dn_d}{da_d} da_d d\nu + k_{\text{CMB}} \\ \Lambda &= \int \int 4\pi^2 a_d^2 B_\nu(T_{\text{dust}}) Q(a_d, \nu) \frac{dn_d}{da_d} da_d d\nu, \end{aligned} \quad (4)$$

where J_ν and k_{CMB} are the mean intensity of stellar radiation and the heating term by CMB radiation, respectively. We simplify the right side of this equation as follows (e.g., Evans 1994),

$$\int \int 4\pi^2 a_d^2 B_\nu(T_{\text{dust}}) Q(a_d, \nu) \frac{dn_d}{da_d} da d\nu \sim 4\pi^2 \bar{a}_d^2 n_d \bar{Q} \sigma T_{\text{dust}}^4, \quad (5)$$

where σ is the Stefan-Boltzmann constant, \bar{a}_d is the mean dust size weighted by the size distribution function,

$$\bar{a}_d = \frac{\int a_d \frac{dn_d}{da_d} da_d}{\int \frac{dn_d}{da_d} da_d}. \quad (6)$$

The \bar{Q} is a mean Q -value weighted by the Planck function,

$$\bar{Q}(T_{\text{dust}}) = \frac{\int B_d(T_{\text{dust}}, \nu) Q(\bar{a}_d, \nu) d\nu}{\int B_d(T_{\text{dust}}, \nu) d\nu}. \quad (7)$$

Then, we obtain the dust temperature by

$$T_{\text{dust}} = \left(\frac{\Gamma}{4\pi^2 \bar{a}_d^2 n_d \bar{Q} \sigma} \right)^{1/4}. \quad (8)$$

3 RESULTS

3.1 Evolution of dust component

In Figure 3, we present the time variation of dust component as a function of the galactic evolution time. Figure 3(a) shows the dust-to-gas mass ratio (D). The ratio increases monotonically with the galaxy evolution owing to continuous supernovae. D is 4×10^{-4} (corresponding to the metallicity $Z = 4 \times 10^{-2} Z_\odot$, where Z_\odot is the solar metallicity) at 0.1 Gyr and reaches 0.7×10^{-2} ($Z = 0.7 Z_\odot$) at 1.0 Gyr .

Figure 3(b) shows the total dust mass in the model galaxy. The dust mass is $1.6 \times 10^7 M_\odot$ at 0.1 Gyr , and then $(6-7) \times 10^7 M_\odot$ at $\geq 0.3 \text{ Gyr}$. In contrast to the monotonic increase of metallicity, the total dust mass does not change greatly at $\geq 0.3 \text{ Gyr}$. This trend comes from the fact that the continuous energy input by multiple supernovae results in the blowout of dusty gas from the halo. The fraction of escaped gas to the initial amount becomes ~ 50 per cent at $t_{\text{age}} = 1.0 \text{ Gyr}$.

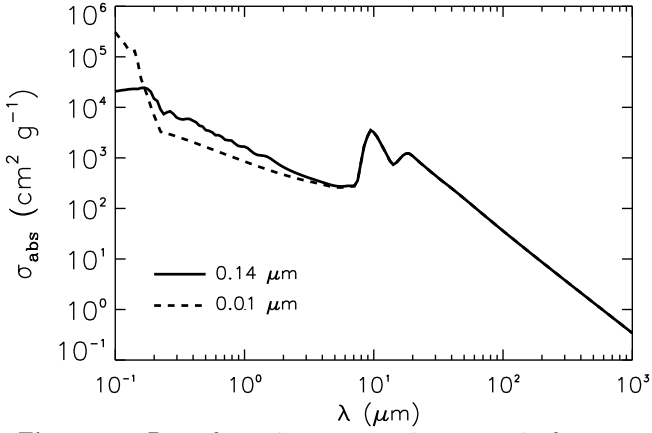


Figure 1. Dust-absorption cross-section per unit dust mass. Solid and dash lines show the cross section of $0.14 \mu\text{m}$ and $0.01 \mu\text{m}$ silicate dust, respectively. The Q-value of silicate dust is taken from Draine & Lee (1984).

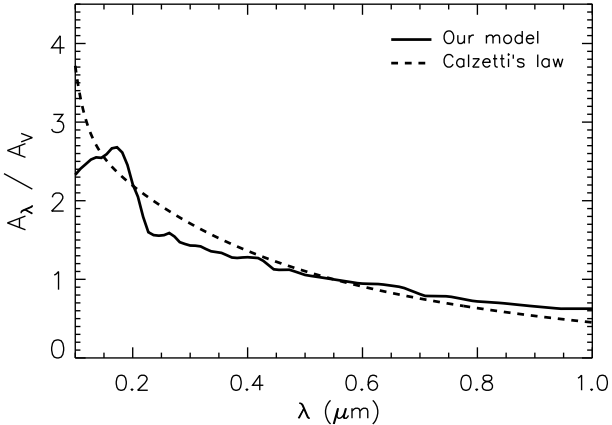


Figure 2. The dust extinction curve. Solid and dash lines show the dust model in this paper and Calzetti's law (Calzetti et al. 2000), respectively.

Our model shows that the metallicity reaches the level of $0.2Z_\odot < Z < 0.4Z_\odot$ in the late phase of LAE. Very recently, Nakajima et al. (2011) assessed the metallicity of LAEs to be $Z \gtrsim 0.16Z_\odot$, which is significantly higher than was previously thought for LAEs. This is concordant with our results.

Figure 3(c) shows the radiation energy absorbed by dust, and Figure 3(d) shows the absorbed fraction to the total radiation energy emitted by stars. The model galaxy has a blue SED owing to young stars, and the absorption efficiency by dust decreases steeply with increasing wavelength. Thus, most of energy absorbed by dust is attributed to UV-optical continuum radiation from stars in the range of $\lambda \sim 1000 - 6000 \text{ \AA}$, and strongly depends on SFR and dust amount. Figure 3(c) shows that the absorbed energy by dust is peaked at 0.3 Gyr, although the metallicity increases monotonically. This is because the dust is distributed compactly around star forming regions in an early phase, and hence the UV photons from stars are effectively absorbed.

3.2 Dust temperature

Figure 4 shows the dust temperature distributions, when the model galaxy is placed at $z = 3$. The dust temperature is $T_{\text{dust}} \sim 35 \text{ K}$ near star-forming regions, while $T_{\text{dust}} \sim 10 \text{ K}$ far from there. In an early phase ($t_{\text{age}} = 0.1 - 0.3 \text{ Gyr}$), the high-temperature regions are distributed extensively according to the distributions of star-forming regions. In a later phase ($t_{\text{age}} = 0.5 - 1.0 \text{ Gyr}$), the distributions of high-temperature dust are confined into the central regions as a result of the dynamical evolution of star-forming regions.

We statistically study the dust temperature distributions. Figure 5 shows the mass fraction of dust in a given temperature range. In an early stage, dust is confined in each sub-halo, and therefore it is distributed near star-forming regions. Thus, at $t_{\text{age}} = 0.1 \text{ Gyr}$, a part of dust has high temperature of $T_{\text{dust}} \geq 35 \text{ K}$, and the mass fraction is broadly distributed in the range of $T_{\text{dust}} = 10 - 40 \text{ K}$. Thereafter, the dusty gas is blown away by supernova explosions and is distributed diffusely in the extended regions. Then, a part of dust, which is far from young stars, cannot absorb much radiation energy, and therefore becomes in a cooler state. Hence, in a later phase, dust with high temperature of $T_{\text{dust}} \geq 35 \text{ K}$ disappears, and the dust temperature falls in the range of $T_{\text{dust}} \approx 10 - 30 \text{ K}$.

Figure 6 shows the mean temperature as a function of evolution time. Filled and open circles are the mass weighted mean temperatures and the energy weighted ones, respectively. The mass weighted mean is $\sim 24 \text{ K}$ in the LAE phase, while $\sim 20 \text{ K}$ in the LBG phase. The energy weighted mean is $\sim 31 \text{ K}$ in the LAE phase, while $\sim 26 \text{ K}$ in the LBG phase. The high-temperature dust emits thermal radiation more effectively than colder one owing to the higher Q-value and the strong temperature-dependence of emissivity. Hence, the energy weighted mean temperatures are higher by $\sim 5 \text{ K}$ than the mass weighted ones. The mean temperatures decline with the evolution time especially in early phases. This is intimately relevant to the sub-mm brightness of the galaxy. Recently, Hwang et al. (2010) have studied the dust properties of galaxies with $L_{\text{IR}} = 10^{11} L_\odot$ in the redshift range $0.1 \lesssim z \lesssim 2.8$, and found the dust temperature to be $T_{\text{dust}} \sim 20 - 50 \text{ K}$. Amblard et al. (2010) have found that the average dust temperature is $28 \pm 8 \text{ K}$ for submm galaxies with the average redshift of 2.2 ± 0.6 . These temperatures are comparable to the dust temperature in our calculations.

3.3 Spectral Energy Distributions

We compute the intrinsic spectral energy distributions (SED) of the stellar component in the model galaxy by using the population synthesis code PÉGASE v2.0 (Fioc & Rocca 1997). We place the model galaxy at several redshifts. The initial mass function (IMF) is assumed to be that by Salpeter (1955) in the mass range of $0.1 - 50 M_\odot$. Also, the effects by the age and metallicity of stellar population are incorporated by interpolating the table generated by PÉGASE. The dust temperature is primarily determined by the UV continuum from OB stars with $\gtrsim 2 M_\odot$. For the Salpeter IMF in the range of $0.1 - 50 M_\odot$, the mass fraction of stars with $\gtrsim 2 M_\odot$ is 0.267. If we suppose the range of $0.1 - 100 M_\odot$, the fraction is 0.287. Hence, the upper bound of mass range is not so significant on determining the dust temperature.

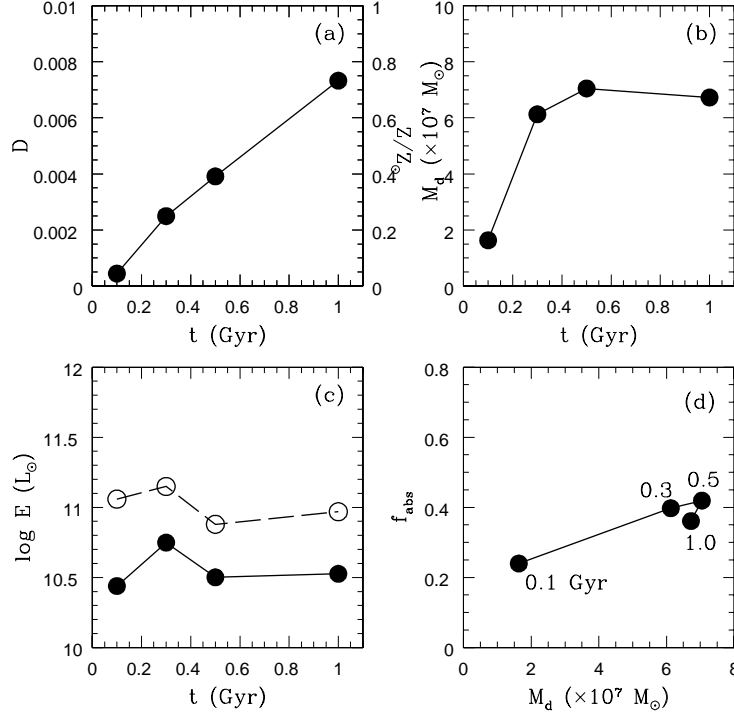


Figure 3. *upper left* : Dust-to-gas mass ratio as a function of evolution time. *upper right* : Total dust mass as a function of evolution time. The dust mass is estimated in proportion to metallicity. *lower left* : Radiation energy absorbed by dust as a function of evolution time (filled circles). Open circles are intrinsically radiated energy from stars. *lower right* : The absorbed fraction to the total radiated energy as a function of the dust mass.

In this work, at first, we derive the intrinsic SED of stellar component by PÉGASE, and correct the SED by incorporating the dust extinction through three-dimensional RT simulations. Then, we evaluate the dust temperature and the thermal emission following the equation (7). Finally, we get the emergent SED by combining the dust absorption-corrected stellar SED with the thermal emission from dust. Fig. 7 shows the resultant SED of the model galaxy in the observed frame after making the K-correction. As well known, $\lambda \gtrsim 1$ mm, the flux density does not decrease with redshift owing to the effect of negative K-correction.

3.4 Sub-millimeter brightness

Here, we see the time variations of the sub-millimeter brightness, focusing on the flux at $850 \mu\text{m}$. Figure 8 shows the total flux at $850 \mu\text{m}$ in observed frame (S_{850}). Interestingly, the sub-millimeter brightness is peaked at 0.3 Gyr (LAE phase), independent of the assumed redshift. As already shown in Figure 3(a), the dust-to-gas ratio (metallicity) increases monotonically with time. But, the sub-millimeter brightness does not increase according to the increase of metallicity. This is because, in the LAE phase, dust grains are concentrated on clumpy star-forming regions and therefore the dust grains can be effectively heated up by stellar radiation. On the other hand, the continuous supernovae drive dust grains far away from star-forming regions at ≥ 0.5 Gyr (LBG phase). Then the grains cannot absorb much ra-

diation from stars and turn into a cold state. As a result, the sub-millimeter brightness declines.

The relative sub-millimeter flux at each epoch depends on the redshift z . If the galaxy is at $z \lesssim 3$, the total flux at 0.1 Gyr is smaller than that at 0.5 Gyr and 1.0 Gyr, although the total absorbed energy is nearly equal. This is due to the fact that the flux of $850 \mu\text{m}$ is sensitive to the dust temperature. The spectral shape of dust emission is basically that of the black body, although the Q -value affects the shape to some degree. The temperature, which exhibits a peak at $850 \mu\text{m}$ in the observed frame, is 13.65 K for a galaxy at $z = 3$. As seen in Figure 6, the mass-weighted mean temperature declines with the evolution time, and the temperature at 0.5 Gyr and 1.0 Gyr is closer to 13.65 K than that at 0.1 Gyr. Therefore, we conclude that the low sub-mm flux in an earlier LAE phase is not attributed to the low dust amount but rather to the higher dust temperature. For higher galaxy redshifts, the absolute flux decreases of course with increasing redshift. But, the difference of the flux between 0.1 and 0.5 (or 1.0) Gyr becomes smaller, since the $850 \mu\text{m}$ in the observed frame is corresponding to shorter wavelengths.

4 DETECTABILITY BY ALMA

Here, we assess the feasibility to detect early star-forming galaxies with SFR of $\sim 10 M_\odot \text{ yr}^{-1}$ by *Atacama Large Millimeter/submillimeter Array* (ALMA). In the present sim-

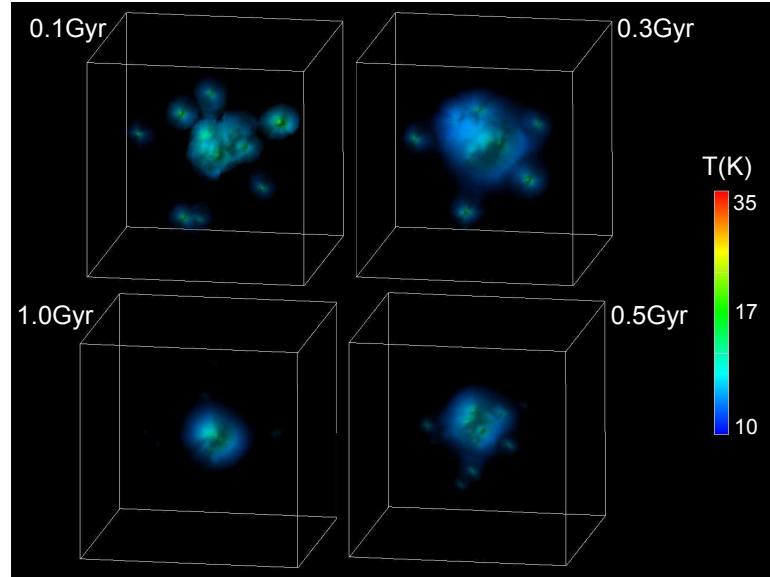


Figure 4. The distributions of dust temperature when the model galaxy is placed at $z = 3$. The color shows dust temperature.

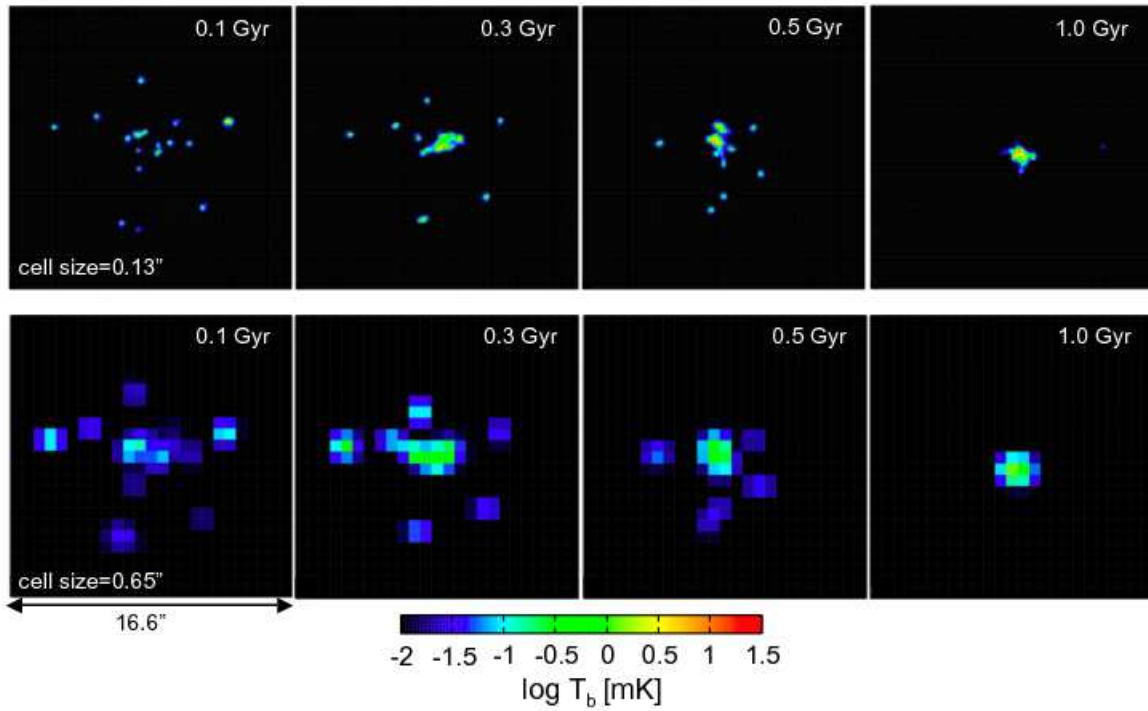


Figure 9. The map of brightness temperature at $\lambda = 850 \mu\text{m}$ in the model galaxy, assuming the galaxy to be located at $z = 3$. The linear scale of each panel is $16.6''$. Upper panels show the map with the original spatial resolution which corresponds to the angular resolution of $0.13''$. Lower panels are the map coarse-grained with the angular resolution of $0.65''$.

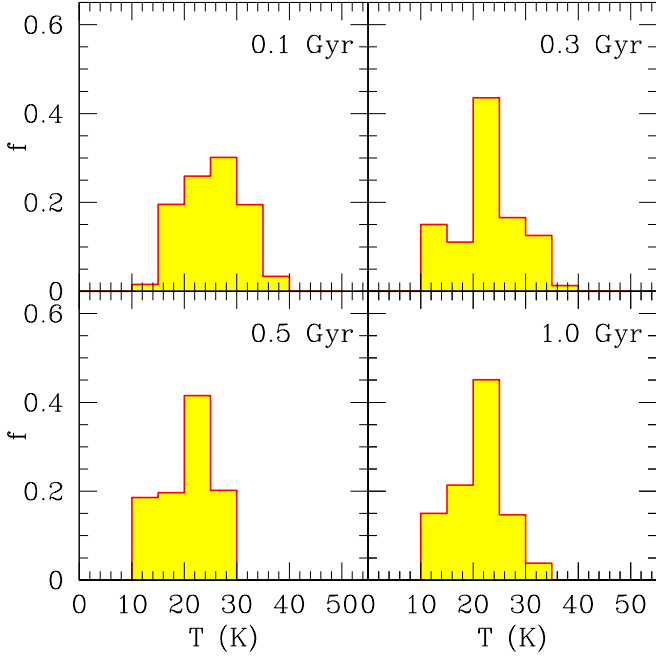


Figure 5. Mass fraction of dust to the total amount in a given temperature range. The bin size is 5 K.

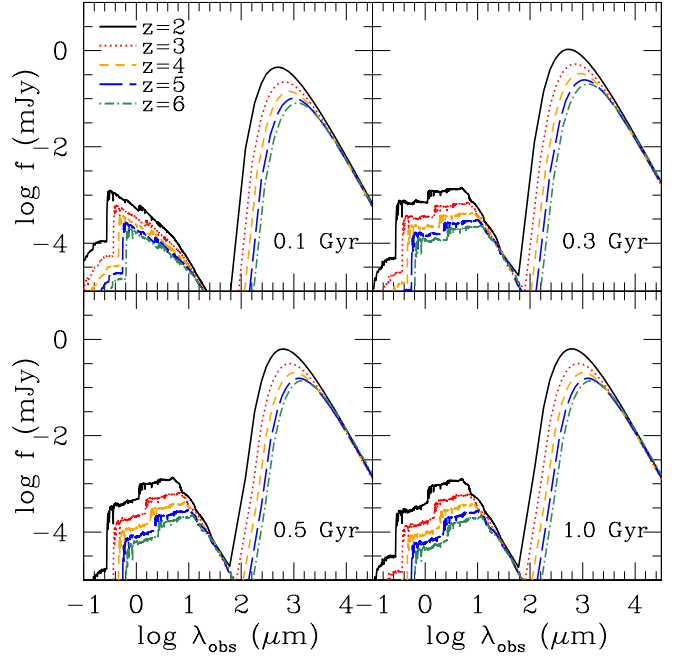


Figure 7. Spectral energy distributions of the model galaxy in the observed frame after the K-correction is made. Different line style corresponds to a different redshift at which the model galaxy is placed (solid: $z = 2$, dot: $z = 3$, dash: $z = 4$, long-dash: $z = 5$ and dot-dash: $z = 6$).

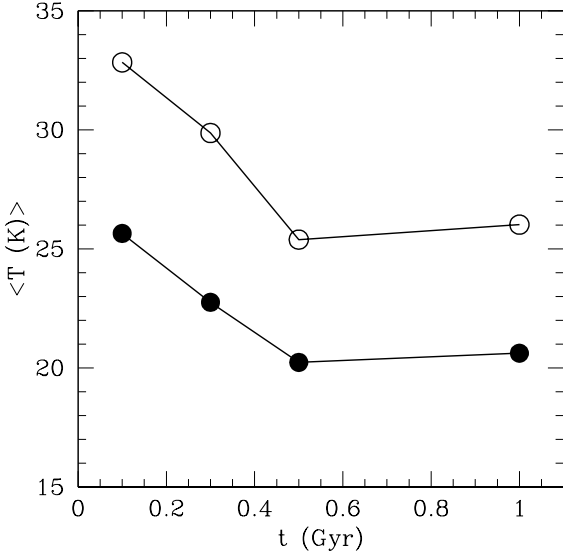


Figure 6. The mean temperature of dust as a function of evolution time. Open and filled circles are the energy weighted mean and the mass weighted mean, respectively.

ulation, the total flux of $850 \mu\text{m}$ in the LBG phase is $S_{850} = 0.65 \sim 0.3 \text{ mJy}$ for a galaxy at $z = 3$. Some lensed LBGs have been detected at sub-millimeter, and show $S_{850} = 0.40 \text{ mJy}$ and $SFR \sim 10 M_{\odot} \text{ yr}^{-1}$ at $z = 2.9$ (MS0451-a : Borys et al. 2004), $S_{850} = 0.39 \text{ mJy}$ and $SFR \sim 24 M_{\odot} \text{ yr}^{-1}$ (cB58 : Baker et al. 2004), or $S_{850} = 0.65 \text{ mJy}$ and $SFR \sim 9 M_{\odot} \text{ yr}^{-1}$ at $z = 2.5$ (SMMJ16359

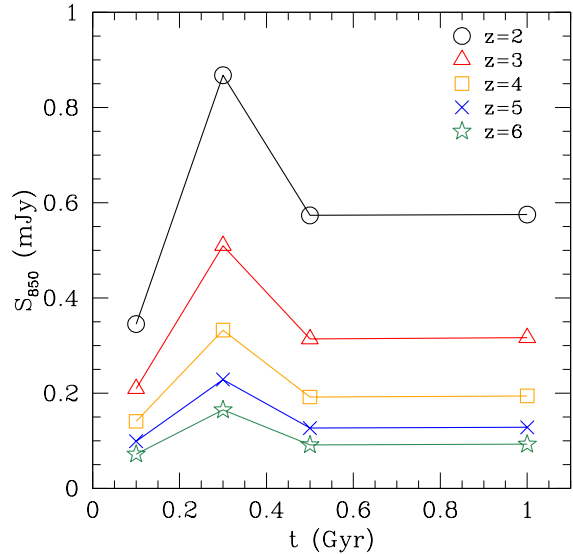


Figure 8. Total flux at $850 \mu\text{m}$ in the observed frame as a function of evolution time. We set the model galaxy at each redshift (circle: $z = 2$, triangle: $z = 3$, square: $z = 4$, cross: $z = 5$ and star: $z = 6$).

: Kneib et al. 2005). Our results match these observations well. Also, Stanway et al. (2010) showed the upper limit of sub-millimeter flux, $S_{870} < 0.85$ mJy, for LBGs at $z = 5$. Our prediction is under their upper limit, and therefore higher sensitivity is required to detect sub-mm flux from LBGs at $z \gtrsim 5$. On the other hand, there are a few bright LBGs detected at sub-millimeter which show $S_{850} \sim 1 - 5$ mJy and $SFR \sim 100 - 200 M_{\odot} \text{ yr}^{-1}$ (Belokurov et al. 2007; Coppin et al. 2007; Chapman & Casey 2009). These may be more massive and dusty star-burst systems.

In Fig. 9, the map of the brightness temperature at $\lambda = 850 \mu\text{m}$ is shown for the model galaxy placed at $z = 3$. The brightness temperature T_b is given by

$$T_b = 11.2 \left(\frac{\lambda}{850 \mu\text{m}} \right)^2 \left(\frac{\theta^2}{1'' \times 1''} \right)^{-1} \left(\frac{F}{\text{mJy}} \right) \text{mK}. \quad (9)$$

The higher T_b traces the star-forming regions. Clumpy clouds with higher T_b are distributed over an extended area in the LAE phase ($t_{\text{age}} = 0.1 - 0.3$ Gyr), while those are concentrated near the center in the LBG phase ($t_{\text{age}} = 0.5 - 1.0$ Gyr).

The upper panels in Figure 9 show T_b in the original resolution of simulations that corresponds to $\theta \sim 0.13''$. The model galaxy exhibits $T_b \sim 0.1 - 40$ mK, where the high T_b regions are of $\gtrsim 20$ mK. The integration time required to detect extended sources of ~ 20 mK with the angular resolution of $\theta \sim 0.13''$ is assessed to be ~ 5 hours per each beam. The sub-millimeter flux strongly correlates with the stellar distribution. At an early phase, the area to cover the half mass of stars is $\sim 13 \text{ arcsec}^2$. At a later phase, the model galaxy becomes as compact as $\sim 4 \text{ arcsec}^2$. Hence, the number of beams to cover the area will be quite large. Even for the later compact phase, the required time to cover the area will be a few hundred hours. Thus, the observations with the angular resolution of $\sim 0.13''$ do not seem achievable to trace the sub-mm structure for early star-forming galaxies.

The lower panels of Figure 9 show T_b in the coarse-grained resolution of $\theta \sim 0.65''$. The high T_b regions show $\gtrsim 3$ mK. In such an angular resolution, the sensitivity with 16 antennas of ALMA is ~ 2 mK by ~ 60 minute integration. If an early star-forming galaxy is observed, some beams may detect sub-mm flux by the integration of less than 1 hour. Thus, the detection of clumpy sub-mm features of an early star-forming galaxy seems feasible. Moreover, observations with lower angular resolution of $\gtrsim 1''$ allow us to study the statistics of high- z sub-mm sources, e.g., the luminosity function of sub-mm galaxies. ALMA will detect the sub-millimeter flux from LBGs at $z \sim 3$ by ~ 10 minute integration with 16 antennas. Even for a galaxy at $z = 6$, ALMA can detect it by ~ 60 minute integration.

Recently, Dayal et al. (2011) have estimated a bit lower flux at $850 \mu\text{m}$ than the present prediction. They have assumed homogeneous distributions of stars and dust for an LAE identified in a cosmological simulation. Compared to our results, it implies that the clumpiness of star-forming regions and interstellar medium significantly contributes to the enhancement of the sub-mm brightness.

5 SUMMARY

We have performed three-dimensional radiative transfer calculations on high-resolution hydrodynamic simulations with inhomogeneous metal enrichment. Then, we have explored the dust temperature and sub-mm flux in a high-redshift star-forming galaxy. Attention has been concentrated on the sub-mm properties of LAE and LBG phases. The star formation rate (SFR) is $\sim 10 M_{\odot} \text{ yr}^{-1}$ in the LAE phase, and several $M_{\odot} \text{ yr}^{-1}$ in the LBG phase. As a result, we have found that dust grains concentrated on clumpy star-forming regions can effectively absorb UV radiation from stars in the LAE phase, and then the grains are heated up to $T_{\text{dust}} \gtrsim 35$ K. On the other hand, in the LBG phase, the continuous supernovae blow away dusty gas from star-forming regions. Hence, the grains cannot absorb much radiation from stars and turn into a cold state. Resultantly, the emergent sub-millimeter brightness is peaked in an LAE phase around $t_{\text{age}} \sim 0.3$ Gyr, independent of the assumed redshift. This shows that the sub-millimeter brightness does not necessarily increase according to the increase of the dust-to-gas ratio or the metallicity. We have found that the clumpiness of star-forming regions and interstellar medium significantly enhances the sub-mm brightness.

Also, by deriving the spectral energy distributions, we have assessed the flux at $850 \mu\text{m}$. The flux is found to be $S_{850} \sim 0.2 - 0.9$ mJy, if the model galaxy is placed at $6 \geq z \geq 2$. Even for $z = 6$, the sub-mm flux does not decrease largely because of negative K-correction. With angular resolution of $\theta \sim 0.65''$, ALMA can detect the sub-mm flux from an LAE as well as an LBG by the integration of less than 1 hour with 16 antennas. Observations with angular resolution of $\gtrsim 1''$ allow us to detect high- z sub-mm sources by ~ 10 minute integration with 16 antennas of ALMA. Therefore, we can study clumpy sub-mm features of an early star-forming galaxy and also the statistics of the luminosity function of sub-mm galaxies with ALMA.

ACKNOWLEDGMENTS

We are grateful to K. Nagamine, A. Inoue, Y. Miyamoto and M. Ouchi for valuable discussion and comments. We thank the anonymous referee for useful comments. Numerical simulations have been performed with the *FIRST* simulator and *T2K-Tsukuba* at Center for Computational Sciences, in University of Tsukuba. This work was supported in part by the *FIRST* project based on Grants-in-Aid for Specially Promoted Research by MEXT (16002003) and JSPS Grant-in-Aid for Scientific Research (S) (20224002), (A) (21244013), and (C) (18540242).

REFERENCES

- Amblard A., et al., 2010, A&A, 518, L9+
- Austermann J. E., et al., 2010, MNRAS, 401, 160
- Barger A. J., Cowie L. L., Sanders D. B., Fulton E., Taniguchi Y., Sato Y., Kawara K., Okuda H., 1998, Natur, 394, 248
- Baker, A. J., Tacconi, L. J., Genzel, R., Lehnert, M. D., Lutz, D., 2004, ApJ, 604, 125
- Belokurov, V., 2007, ApJ, 671, L9

- Bertoldi F., et al., 2007, *ApJS*, 172, 132
- Bianchi S., Schneider R., 2007, *MNRAS*, 378, 973
- Borys C., et al., 2004, *MNRAS*, 352, 759
- Borys C., Chapman S., Halpern M., Scott D., 2003, *MNRAS*, 344, 385
- Calzetti, D., Armus, L., Bohlin, R. C., Kinney, A. L., Koornneef, J., Storchi-Bergmann, T., 2000, *ApJ*, 533, 682
- Chapman S. C., Blain A. W., Smail I., Ivison R. J., 2005, *ApJ*, 622, 772
- Chapman, S. C. and Casey, C. M., 2009, *MNRAS*, 398, 1615
- Coppin K., et al., 2006, *MNRAS*, 372, 1621
- Coppin, K. E. K., et al., 2007, *ApJ*, 665, 936
- Daddi E., et al., 2009, *ApJ*, 694, 1517
- Dayal P., Hirashita H., Ferrara A., 2010, *MNRAS*, 403, 620
- Draine B. T., Lee H. M., 1984, *ApJ*, 285, 89
- Draine B. T., et al., 2007, *ApJ*, 663, 866
- Dwek E., 1998, *ApJ*, 501, 643
- Eales S., Lilly S., Gear W., Dunne L., Bond J. R., Hammer F., Le Fèvre O., Crampton D., 1999, *ApJ*, 515, 518
- Eales S. A., et al., 2010, *A&A*, 518, L23
- Evans A., 1994, *The dusty universe*, Evans, A., ed.
- Eyles, L. P., Bunker, A. J., Ellis, R. S., Lacy, M., Stanway, E. R., Stark, D. P., Chiu, K., 2007, *MNRAS*, 374, 910
- Fioc M., Rocca V. B., 1997, *A&A*, 326, 950
- Greve T. R., Ivison R. J., Bertoldi F., Stevens J. A., Dunlop J. S., Lutz D., Carilli C. L., 2004, *MNRAS*, 354, 779
- Hatsukade B., et al., 2011, *MNRAS*, 411, 102
- Hughes D. H., et al., 1998, *Nature*, 394, 241
- Hwang H. S. et al., 2010, *MNRAS*, 409, 75
- Ivison R. J., Smail I., Barger A. J., Kneib J.-P., Blain A. W., Owen F. N., Kerr T. H., Cowie L. L., 2000, *MNRAS*, 315, 209
- Kneib J., Neri R., Smail I., Blain A., Sheth K., van der Werf P., Knudsen K. K., 2005, *A&A*, 434, 819
- Laurent G. T., et al., 2005, *ApJ*, 623, 742
- Mathis J. S., Rumpl W., Nordsieck K. H., 1977, *ApJ*, 217, 425
- Mori M., Umemura M., 2006, *Nature*, 440, 644
- Nakajima K., et al., 2011, *ArXiv e-prints*
- Nakamoto T., Umemura M., Susa H., 2001, *MNRAS*, 321, 593
- Nozawa T., Kozasa T., Habe A., 2006, *ApJ*, 648, 435
- Nozawa T., Kozasa T., Habe A., Dwek E., Umeda H., Tomimaga N., Maeda K., Nomoto K., 2007, *ApJ*, 666, 955
- Perera T. A., et al., 2008, *MNRAS*, 391, 1227
- Salpeter E. E., 1955, *ApJ*, 121, 161
- Scott K. S., et al., 2008, *MNRAS*, 385, 2225
- Smail I., Ivison R. J., Blain A. W., 1997, *ApJ*, 490, L5
- Stanway E. R., Bremer M. N., Davies L. J. M., Lehnert M. D., 2010, *MNRAS*, 407, L94
- Stark, D. P., Ellis, R. S., Bunker, A., Bundy, K., Targett, T., Benson, A., Lacy, M., 2009, *ApJ*, 697, 1493
- Takagi T., Vansevicius V., Arimoto N., 2003, *PASJ*, 55, 385
- Tamura Y., et al., 2009, *Nature*, 459, 61
- Todini P., Ferrara A., 2001, *MNRAS*, 325, 726
- Verma, A., Lehnert, M. D., Förster Schreiber, N. M., Bremer, M. N., Douglas, L., 2007, *MNRAS*, 377, 1024
- Weiß A., et al., 2009, *ApJ*, 707, 1201
- Yajima H., Umemura M., Mori M., Nakamoto T., 2009, *MNRAS*, 398, 715
- Yajima, H., Choi, J.-H., Nagamine, K., 2011, *MNRAS*, 412, 411